

HI in Virgo's "Red and Dead" Dwarf Ellipticals— A Tidal Tail and Central Star Formation

Gregory Hallenbeck^{1,2}, Rebecca Koopmann¹, Riccardo Giovanelli³, Martha P. Haynes³, Shan Huang⁴, Lukas Leisman³, and Emmanouil Papastergis⁵ Union College, Department of Physics & Astronomy, 807 Union Street, Schenectady NY 12308, USA; hallenbg@union.edu, koopmanr@union.edu ² Washington & Jefferson College, Department of Computing and Information Studies, 60 S Lincoln Street, Washington PA 15301, USA Cornell Center for Astrophysics and Planetary Science (CCAPS), Space Sciences Building, Cornell University, Ithaca, NY 14853, USA; riccardo@astro.cornell.edu, haynes@astro.cornell.edu, leisman@astro.cornell.edu CCPP, New York University, 4 Washington Place, New York, NY 10003, USA; shan.huang@nyu.edu ⁵ Kapteyn Astronomical Institute, University of Groningen, Landleven 12, Groningen NL-9747AD, The Netherlands; papastergis@astro.rug.nl Received 2017 March 5; revised 2017 May 27; accepted 2017 June 25; published 2017 July 20

Abstract

We investigate a sample of three dwarf elliptical galaxies in the Virgo Cluster that have significant reservoirs of HI. We present deep optical imaging (from CFHT and KPNO), HI spectra (Arecibo), and resolved HI imaging (VLA) of this sample. These observations confirm their H I content and optical morphologies, and indicate that the gas is unlikely to be recently accreted. The sample has more in common with dwarf transitionals, though dwarf transitionals are generally lower in stellar mass and gas fraction. VCC 190 has an H I tidal tail from a recent encounter with the massive spiral galaxy NGC 4224. In VCC 611, blue star-forming features are observed that were not seen by shallower SDSS imaging.

Key words: galaxies: clusters: individual (Virgo) – galaxies: evolution – galaxies: individual (VCC 190, VCC 611, VCC 1533)

1. Introduction

The relationship between gas-rich late-type dwarfs—irregulars and blue compact dwarfs (BCDs)—and early-type dwarfs —dwarf ellipticals and spheroidals—is unclear. Are late-type dwarfs the progenitors of early-types, or are the two populations largely distinct, with late-types evolving in the field and dwarf ellipticals in cluster environments? On one hand, many early-type dwarfs show late-type features: faint disk-like structures (Lisker et al. 2006b; Penny et al. 2014), rotational support (Beasley et al. 2009; Guérou et al. 2015; Toloba et al. 2016), and lingering central star formation (Lisker et al. 2006a; De Looze et al. 2013). In turn, the underlying old stellar population of late-type dwarfs resemble dwarf ellipticals and spheroidals (Meyer et al. 2014). On the other hand, simulations (Weinmann et al. 2011; Lisker et al. 2013; Mistani et al. 2016) and stellar population modeling (Rakos & Schombert 2004; Koleva et al. 2009; Paudel et al. 2010; Roediger et al. 2011; Weisz et al. 2014; Guérou et al. 2015) suggest that early-type dwarfs essentially halted star formation at $z \sim 1$, and so late-type dwarfs at z = 0 are unlike their progenitors.

Essentially, all dwarfs in the field are star-forming or in a starburst phase (Lee et al. 2009; Geha et al. 2012), while quiescent dwarf ellipticals predominate in the cluster (Dressler 1980; Binggeli et al. 1987). If these populations are related, then it is assumed that the cluster environment is responsible for this transformation. As gas-rich late-type galaxies fall onto the cluster, their gas is removed via processes such as ram-pressure stripping (Boselli et al. 2008; Boselli et al. 2016) or galaxy harassment (Mayer et al. 2001; Aguerri & González-García 2009). This process is relatively rapid, less than 100 Myr (Boselli et al. 2008). By the time a dwarf galaxy has crossed through the cluster core,

they are almost entirely gas free (>99% gas removed). Without gas, star formation ceases, the galaxy's colors redden, and it loses any irregular or spiral features, becoming a smooth dwarf elliptical.

Given that gas removal precedes morphological changes, there should be few, if any, dwarf elliptical galaxies that still have a detectable reservoir of H I. Furthermore, there are indeed only a few, about 2%, that do (e.g., Huchtmeier & Richter 1986; di Serego Alighieri et al. 2007; Taylor et al. 2012). In the work of Hallenbeck et al. (2012), hereafter H12, we identified a sample of seven gas-bearing dwarf elliptical galaxies in the Virgo Cluster. The star formation in this sample is clearly suppressed: the galaxies are as red as typical dwarf ellipticals in the g - i, NUV-r, and FUV-r bands. Additionally, their gas fractions (GF $\equiv M_{\rm H\,I}/M_{*}$) are typical for unstripped dwarfs both in Virgo and the field (Huang et al. 2012). Based on this, we argued that the gas has recently been accreted.

How plausible is this assertion, given their evidence? Most dwarf ellipticals have cluster orbits that are highly radial (Conselice et al. 2001). This means that they will spend most of their time near the cluster edge—which is where the sample preferentially lies—where they can encounter clouds of neutral gas falling onto the cluster. At their present positions outside the X-ray emitting region of Virgo, accretion is possible because the evaporation of clouds of neutral H I due to the hot intracluster medium is relatively slow compared to the time it would take to accrete a cloud of H_I (H12).

The purpose of this work is to test the re-accretion hypothesis of H12, using new deep optical and H I observations. In Section 2, we review and update the sample of H12, removing galaxies whose H I was not confirmed. In Section 3, we present the results of new optical and HI observations of the sample. We weigh the evidence for morphological transformation of the galaxies in

Table 1
Sample Counts

Selection Criteria	Galaxies
Binggeli et al. (1985) (VCC) Galaxies	2096
Dwarfs Ellipticals in Virgo	365
Red dEs with H I Detections (H12)	7
H I Confirmed by Follow-up	5
Removal of VCC 956 and VCC 1993 (see the text)	3

Note. Number of galaxies in the sample after each cut was applied. This work is concerned only with the three that remain after all cuts have been applied.

Section 4, for recent accretion in Section 5.1, and for quenched star formation without gas removal in Section 5.2. In Section 6, we argue that VCC 190 has had gas removed via tidal stripping.

2. Sample Selection and Updates

Our sample selection is outlined in Table 1, as well as below. In H12, we defined a sample of dwarf elliptical galaxies in the Virgo Cluster. These galaxies were identified using the morphology and subcluster assignments from the Virgo Cluster Catalog (VCC; Binggeli et al. 1985), updates from (Binggeli et al. 1993), and our own internal assignments.

Of these 365 dwarf ellipticals, 7 had enough H I such that they were detected in the Arecibo Legacy Fast ALFA survey (ALFALFA; Giovanelli et al. 2005; Haynes et al. 2011) and clearly lay along the red sequence (SDSS $g - r \ge 0.45$).

2.1. ALFALFA Follow-up

The H I detections of this sample were often near the detection limit of ALFALFA's, with signal-to-noise ratios of $3 < \mathrm{SN} < 10$. Thus, we re-observed each object as part of a larger ALFALFA campaign to confirm the H I in unusual and low signal-to-noise galaxies.

We performed a 3 minute ON/OFF observation of each galaxy using the single pixel L-Band Wide (LBW) receiver. These pointed observations have an rms of 1.1 mJy in $10\,\mathrm{km\,s^{-1}}$ wide channels, and are thus twice as sensitive as ALFALFA, which has a typical rms of 2.2 mJy when smoothed to the same width.

Out of the seven, the H_I emission in five of the galaxies was confirmed. The two galaxies with the lowest signal-to-noise (VCC 421 and VCC 1649) were not confirmed, and so we remove them from our sample.

2.2. The Trouble with VCC 956 and VCC 1993

Oosterloo & van Gorkom (2005) mapped an H I tail caused by ram-pressure stripping off of NGC 4388, which ranges in velocity from $2000 < v < 2600 \, \mathrm{km \, s^{-1}}$. The sky position of VCC 956 coincides with the end of the tail, as shown in Figure 1. Our nominal H I detection has a velocity of $v = 2200 \, \mathrm{km \, s^{-1}}$, which perfectly coincides with the velocity of NGC 4388's tail at that position (see Oosterloo & van Gorkom 2005, Figures 1 and 2). There are no independent redshift measurements of VCC 956. It is thus likely that our nominal H I measurement of VCC 956 is better identified with the tail of NGC 4388, and we remove it from our sample.

The surface brightness profile of VCC 1993 indicates that it is not a dwarf elliptical, but a low-mass elliptical. It also has the highest M_* in the sample by a factor of 10. So, we remove it

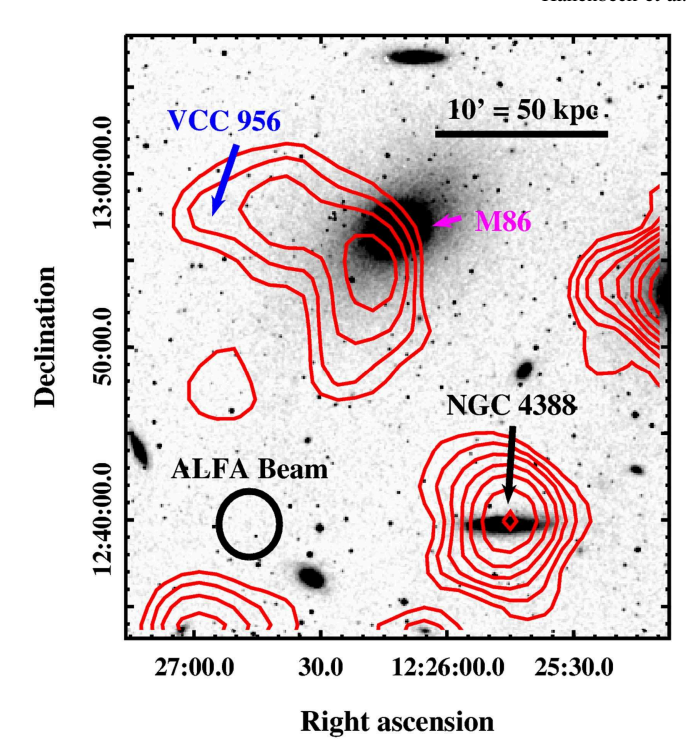


Figure 1. VCC 956 and its local environment. VCC 956 lies along the tidal tail off of NGC 4388, and our H I redshift coincides with the tail redshift of 2200 km s⁻¹. It is thus likely that the H I detected at the sky location of VCC 956 is not associated with the galaxy, and we remove it from our sample. Background is a DSS/II composite optical image, while contours are integrated H I flux from ALFALFA covering 1820 km s⁻¹ < v < 2630 km s⁻¹. Contours are at 4σ (0.6 Jy km s⁻¹ beam⁻¹ = 0.1 M_{\odot} pc⁻²) and increase by a factor of $\sqrt{2}$ at each additional contour. The 3'.8 × 3'.5 ALFA beam is shown for reference.

from the present consideration and focus on the lowest mass, truly dwarf, galaxies.

The remaining three galaxies, VCC 190, VCC 611, and VCC 1533 are the focus of this work.

3. Observations and Results

3.1. Summary of Prior SDSS, GALEX, and ALFALFA Observations

Figure 2 (left) shows an NUV-r color—magnitude diagram of the dwarf sample of H12. Late-type dwarfs with H I are crosses, while early-type dwarfs undetected in ALFALFA are gray dots. The three gas-rich dwarf ellipticals in our sample are plotted as red squares, and labeled with their VCC numbers. With a few exceptions, the late-type and early-type dwarfs separate themselves neatly. From our sample, VCC 190 is unambiguously red in NUV-r color. VCC 611 and VCC 1533 lie in the green valley; while they are redder than almost all of the late-type dwarfs, they are also bluer than most dwarf ellipticals. The galaxies show a similar segregation in FUV-r and g-r colors (see H12; Figure 6).

Figure 2 (right) shows the H I gas fraction as a function of stellar mass of late-type dwarfs (crosses) along with a best-fit trend. The H I-bearing late-type dwarfs lie along the same line as H I-bearing dwarfs outside of the Virgo Cluster (H12; Huang et al. 2012). This suggests that such galaxies have yet to undergo any significant stripping processes. Red boxes with labels are our sample. All three galaxies lie at or below the line defined by the H I-bearing late-types, but none significantly so.

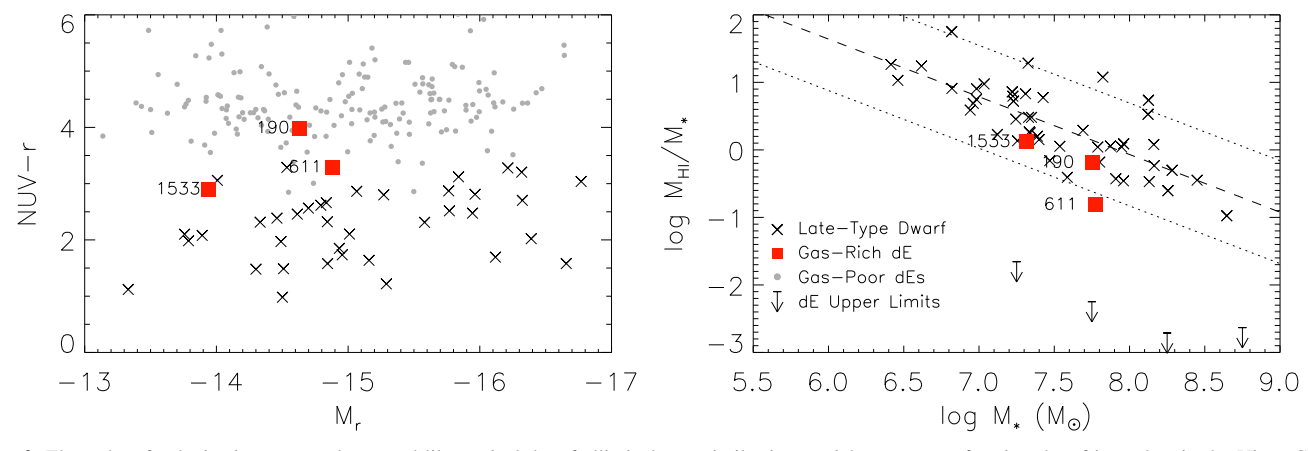


Figure 2. Three dwarf galaxies in our sample are red like typical dwarf ellipticals yet similar in gas richness to star-forming dwarf irregulars in the Virgo Cluster. (Left) Ultraviolet and optical color–magnitude diagram of the dwarf galaxies in the Virgo Cluster. Crosses are late-type dwarfs with gas, gray circles are dwarf ellipticals without gas. Our sample of gas-bearing dwarf ellipticals are labeled with red squares. (Right) Gas fraction as a function of stellar mass for late-type dwarfs and our sample. Lines indicate the best fit and 2σ scatter for the late-type dwarfs, and arrows are the 3σ upper limit for non-detected dwarf ellipticals based on stacking. All measurements are from Huang et al. (2012) with updates in H12.

Arrows are 3σ upper limits on the gas fractions of dwarf ellipticals which were not detected in ALFALFA derived from spectral stacking. The Arecibo Galaxy Environment Survey (AGES; Auld et al. 2006) found similar upper limits over a smaller region of the cluster (Taylor et al. 2012).

The three dwarf ellipticals in our sample thus fall into an unusual class: from their optical and ultraviolet magnitudes alone, they appear to fit in with the dwarf elliptical population by being either "red and dead" (VCC 190), or nearly so (VCC 611 and 1533). However, from their H I gas fractions, they appear to be unstripped late-type dwarfs and several orders of magnitude more gas-rich than other dwarf ellipticals.

3.2. Optical Observations

We obtained optical r-band imaging at the WIYN 0.9 m telescope with the HDI camera at the Kitt Peak National Observatory (KPNO). VCC 190 and VCC 611 were observed for 30 and 36 minutes, respectively, with seeing 1.6. In addition, all three galaxies lay within the footprint of the Next Generation Virgo Survey (NGVS; Ferrarese et al. 2012), performed with the CFHT. All three galaxies were observed between 30 minutes and 1 hr in the u, g, and i bands.

Optical NGVS images of all three galaxies in our sample are shown in Figure 3 (top panels). The three galaxies all appear roughly elliptical but with some peculiar morphology. The highest optical surface density in VCC 190 (top left) is offset from the center, with possible tails to the west and south. The shape of VCC 1533 (right) is boxy, with a nucleated center. Figure 3 (second row) shows r-band (VCC 190 and 611) and i-band (VCC 1533) surface brightness profiles. All three galaxies are well-fit with an exponential profile for r > 5'' (dashed line), consistent with the standard dwarf elliptical profile. At smaller radii, the surface brightness profiles of VCC 1533 are contaminated by what is likely a foreground star.

VCC 611 (top center) appears to be a smooth elliptical, likely due to its relatively higher stellar mass and surface brightness compared with the other two galaxies in our sample. However, it clearly has a very blue center indicative of star formation, which can be seen in Figure 4. The left panel presents an i-band image, which shows a smooth old stellar population. The right panel is a g-i color map of the galaxy, which shows several star-forming knots in the galaxy's center.

VCC 611 was observed as part of the SDSS spectroscopic survey and has H α in emission with an equivalent width (EW) of 25 Å (NASA Sloan Atlas⁶). Lisker et al. (2006b) and Taylor et al. (2012) previously performed unsharp masking on all three of these galaxies using shallower SDSS images, but did not detect the underlying structure or the blue center in VCC 611.

3.3. H I Observations

The H I content of the three dwarf elliptical galaxies in our sample were observed at high spectral resolution (native 0.65 km s⁻¹ channel width) using the Arecibo Observatory. Observations were performed with the LBW receiver in a series of 5 minute ON/OFF pairs. Results are summarized in Table 2. The ALFALFA data cubes indicate that there are no sources within 10' that could be contaminating the sources by being detected in Arecibo's sidelobes above the 5% level.

The H I spectra of the three galaxies are shown in Figure 3 (third row). VCC 611 and VCC 1533 (center and right) are in good agreement with a Gaussian profile: the normalized residuals (bottom center and right) show low scatter and non-significant trends. In addition, we fit third order Gauss-hermite polynomials, to both spectra to look for asymmetric components. For VCC 611, we find no significant asymmetries, while VCC 1533's H I profile is asymmetric at a 3σ level. The velocity widths of both galaxies are very narrow: $W_{50} = 19$ and $28 \, \mathrm{km \, s^{-1}}$, respectively). Fit parameters are presented in Table 2.

The H I profile of VCC 190 (Figure 3; third row left) is neither Gaussian nor does it have a typical symmetric two-horn profile. Attempting to fit a single, asymmetric profile to the galaxy produces a rather poor fit overall ($\chi^2_{\nu} = 3.0$). Such asymmetries in the global H I profile are typical in galaxies for which ongoing ram-pressure stripping is observed (Koopmann & Kenney 2004; Oosterloo & van Gorkom 2005; Chung et al. 2007; Haynes et al. 2007), though stripping is not the only possible explanation.

Instead, guided by our VLA observations (see Section 3.4), we fit two Gaussians, one to the lower redshift peak, and one to the higher redshift peak. The combined model fits the data well ($\chi^2_{\nu} = 1.5$), with no trend in the residuals (bottom left). The

⁶ http://www.nsatlas.org

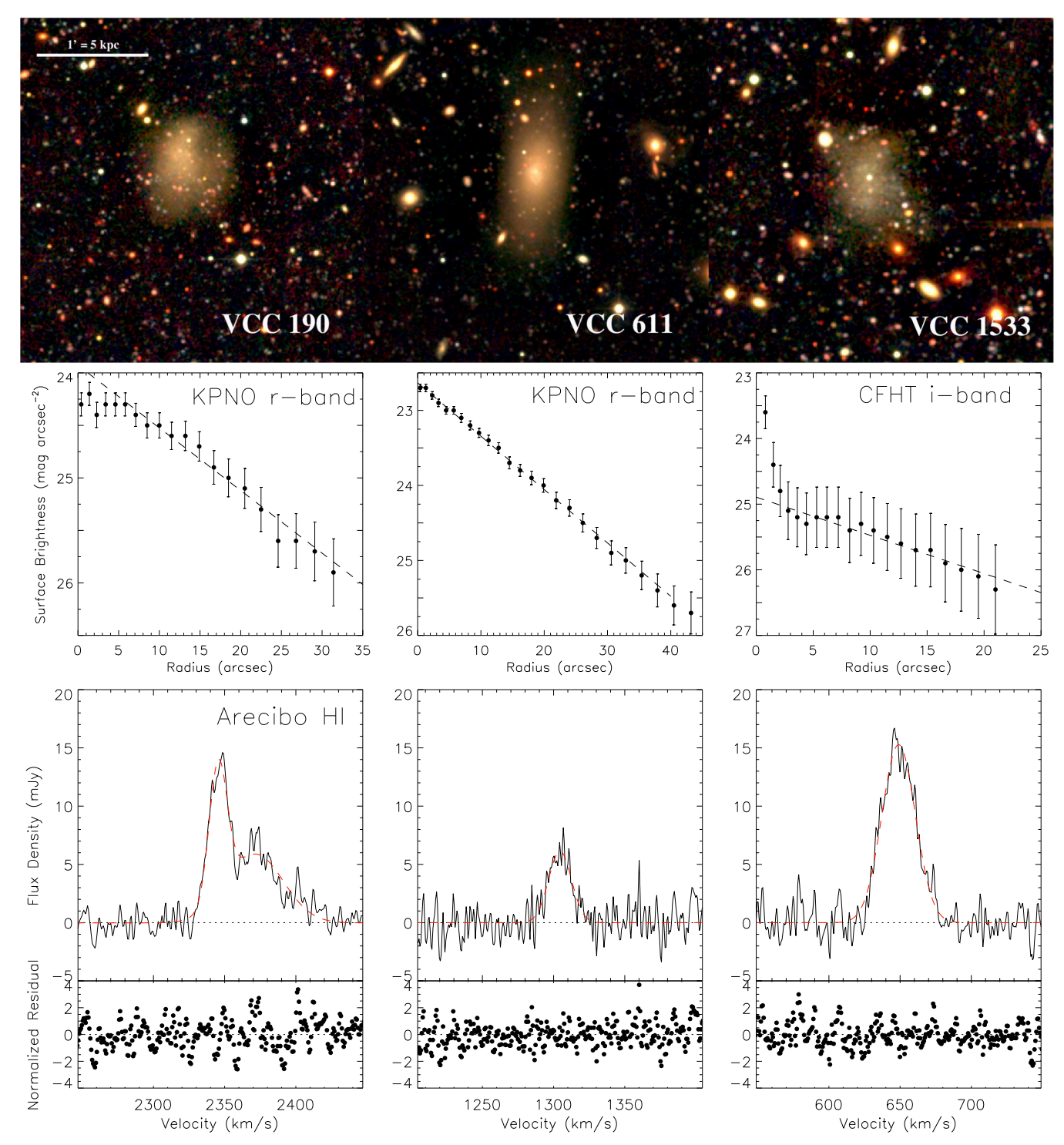


Figure 3. Optical images and H I spectra of our sample of "red and dead" yet gas-bearing dwarf ellipticals. (Top row) Optical CFHT images of the three red dwarf elliptical galaxies in the sample, using u-, g-, and i-band filters. (Second row) Surface brightness profiles of the three galaxies; dashed lines are exponential profiles fit to r > 5". (Third row) H I Spectra; red dashed lines are best-fit Gaussian profiles, except for VCC 190, where two Gaussians are fit. (Bottom row) Normalized residuals from the Gaussian fits. The lack of trend demonstrates that all three galaxies are well described by the fits.

lower redshift peak has a very narrow $W_{50} = 15 \text{ km s}^{-1}$, while the higher redshift peak has $W_{50} = 46 \text{ km s}^{-1}$.

3.4. VLA Observations of VCC 190

We observed VCC 190 using the VLA in the D and C configurations for 2 hr and 4 hr respectively. The cubes were produced in CASA using multiscale clean, with a Briggs

robustness weighting of 1.0. Continuum subtraction was performed in the image plane with the IMCONTSUB task using the line-free channels. This yielded an rms of 1.0 mJy beam $^{-1}$ in a $37''\times31''$ beam, with 7 km s $^{-1}$ wide channels. The moment 0 maps were produced by first smoothing the data cubes to half their original spatial resolution and calculating a mask at 3σ (3.0 mJy beam $^{-1}$). This mask was then applied to the original data cube.

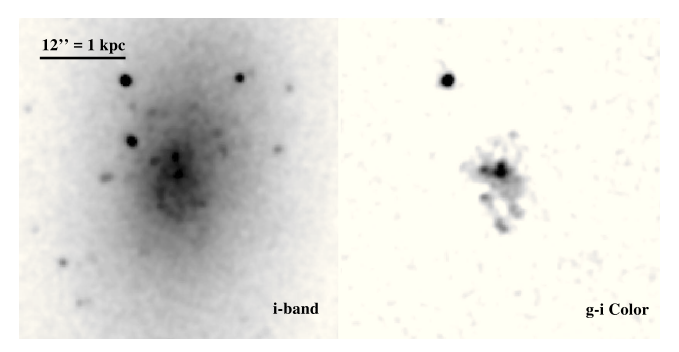


Figure 4. Deep CFHT images reveal that VCC 611 has strong star formation concentrated at the galaxy's center. (Left) CFHT i-band image of the central 4 kpc of VCC 611. (Right) g-i color of the same field. The i-band image shows a mostly smooth old stellar population, while the g-i color shows that star formation is occurring in the galaxy's center, in several star-forming knots.

Figure 5 (left) shows a moment 0 image overlaid on a KPNO r-band optical image. Contours begin at 3σ and increase by 3σ at each additional contour. The gas is not localized directly on the optical, but shows a tail to the southeast. The total flux recovered by the VLA is 0.44 ± 0.01 Jy km s⁻¹, which agrees with the Arecibo flux of 0.47 ± 0.02 Jy km s⁻¹. In Figure 5 (right), we overlay two sets of contours, corresponding to the velocities of the two peaks observed at Arecibo. The blue contours, corresponding to the narrow, lower velocity peak $(2320-2343 \text{ km s}^{-1})$ VCC 190 A roughly coincide with the location of the optical galaxy, with an offset of 12'' = 1 kpc. The red dashed contours correspond to the wider, high velocity peak $(2343-2374 \text{ km s}^{-1})$ VCC 190 B correspond solely to the tail.

4. Galaxy Morphology

In H12, we argued that this sample is morphologically well described as dwarf ellipticals, based on optical morphology and color from relatively shallow imaging. All three galaxies in our refined sample, classified as dwarf ellipticals by Binggeli et al. (1985), are redder than almost all gas-rich late-type dwarfs in the cluster, and no faint substructure was recovered in the galaxies by either Lisker et al. (2006b) or Taylor et al. (2012) using stacked SDSS imaging. Do the new, significantly deeper, optical and H I observations support this assessment?

In the CFHT images, we observe that only VCC 611 appears by eye to be a "typical" dwarf elliptical: it is smooth and clearly elliptically symmetric. VCC 190 and 1533 are a bit peculiar (see Figure 3, first row): VCC 190 is asymmetric and VCC 1533 is boxy in shape. Such peculiar features are, however, not unusual. Massive elliptical galaxies in the field, which are observed to have detectable quantities of H I often have peculiar optical morphology, appearing blue, distorted, or with faint disk-like features (e.g., di Serego Alighieri et al. 2007; Hau et al. 2008; Grossi et al. 2009; Serra et al. 2012).

It is possible that VCC 611 is a massive elliptical galaxy, but appears to be a dwarf because it is behind the cluster. This can be tested using surface brightness profiles: all dwarf galaxies (early- and late-type) are expected to have exponential profiles, as compared with the de Vaucouleurs profile of more massive ellipticals. Using *r*- and *i*-band imaging from KPNO and the CFHT, we observe that exponential profiles do fit all three galaxies very well at radii larger than 5" (see Figure 3, second row). This measure does not, unfortunately, allow us to differentiate between dwarf ellipticals and irregulars.

The bulk motion of stars and gas in dwarf ellipticals is generally not rotational, but pressure-supported. Typical values of $V_{\rm rot} \lesssim \sigma$, where σ is the dispersion velocity. For the stellar component, typical values are $0~{\rm km~s^{-1}} < V_{\rm rot} < 30~{\rm km~s^{-1}}$, while $20~{\rm km~s^{-1}} < \sigma_* < 40~{\rm km~s^{-1}}$ (e.g., van Zee et al. 2004; Ryś et al. 2013; Toloba et al. 2014). This relationship only seems to break down for the most extreme of the so-called fast-rotating and rotationally supported dwarf ellipticals (Beasley et al. 2009).

In agreement with stellar observations of other dwarf ellipticals, all three galaxies in our sample have H I profiles, which show few signs of rotation. All three can be very well fit with a Gaussian profile, with widths of $14 \, \mathrm{km \, s^{-1}} < W_{50} < 28 \, \mathrm{km \, s^{-1}}$ (see Figure 3, bottom two rows). We can estimate a sky-projected rotation velocity via

$$V_{\rm rot} = \frac{\sqrt{W_{50}^2 - \sigma_{\rm H\,I}^2}}{2} \tag{1}$$

where $\sigma_{\rm H\ I}=11\,{\rm km\ s}^{-1}$ is our assumed velocity dispersion, and the factor of two accounts for the integrated spectrum containing both the approaching and receding halves of the rotation curve. We then obtain approximate H I rotational velocities of 4–13 km s⁻¹, or $V_{\rm rot}\lesssim\sigma_{\rm H\ I}$.

By comparison, the estimated rotational velocities for other late-type dwarfs is much higher. For late-type dwarfs in the Virgo Cluster observed by ALFALFA, the average rotational velocity is $31~\rm km\,s^{-1}$, with an interquartile range (IQR) of $18~\rm km\,s^{-1} < V_{\rm rot} < 40~\rm km\,s^{-1}$, several times $\sigma_{\rm H\,I}$. The FIGGS sample of field irregulars (Begum et al. 2008) are typically narrower, with an average $V_{\rm rot}$ of $39~\rm km\,s^{-1}$ (IQR of $11~\rm km\,s^{-1} < V_{\rm rot} < 24~\rm km\,s^{-1}$). While the rotational velocities of the FIGGS sample overlap with our sample, the FIGGS galaxies are also typically of lower mass. Finally, we note that the spectra of most late-type dwarfs in ALFALFA and FIGGS also have a two-horned profile or otherwise show clear features of rotational broadening.

5. Discussion

Thus, our previous assessment that these galaxies are morphologically dwarf ellipticals appears to hold, regardless of whether we consider surface brightness profiles, visual appearance, or velocity widths. There are, however, a few peculiarities that must be explained, primarily their large H I reservoirs in comparison with other dwarf ellipticals. We now explore two hypotheses about the H I content of the galaxies. First, we reconsider the hypothesis of H12 that the gas has been recently accreted. Second, we consider whether these galaxies are a part of the irregular or BCD dwarf population, but are between starburst phases, and so only appear optically red and dead.

5.1. Gas Accretion

Approximately half of giant elliptical galaxies in the field have been observed to bear H I (Morganti et al. 2006; Hau et al. 2008; Grossi et al. 2009; Oosterloo et al. 2010; Serra et al. 2012). In most cases, these authors attributed the presence of gas to accretion—whether of gas-rich satellites, the cooling of ionized gas, or cold-mode accretion from the intergalactic medium (e.g., Struve et al. 2010; Davis et al. 2011; Serra et al. 2012; De Rijcke et al. 2013). However, in clusters, ellipticals do not appear to be accreting (Oosterloo et al. 2010). Morganti

Table 2
Sample H I Properties

Galaxy	Position	$S_{\rm H\ I}$ (Jy km s ⁻¹) (1)	$ \log M_{\rm H I} (\log M_{\odot}) (2) $	V_{sys} (km s^{-1}) (3)	W_{50} (km s ⁻¹) (4)
VCC 190 A	$12^{\rm h}16^{\rm m}26^{\rm s}2 + 07^{\circ}47'39''$	0.18 ± 0.01	7.1	2345.4 ± 0.2	14.9 ± 0.6
VCC 190 B	•••	0.29 ± 0.02	7.3	2371 ± 2	46 ± 2
VCC 611	$12^{\rm h}23^{\rm m}04.8 + 08^{\circ}19'59''$	0.12 ± 0.01	6.9	1304.5 ± 0.6	19 ± 1
VCC 1533	$12^{h}34^{m}02\stackrel{\circ}{.}6 + 05^{\circ}57'49''$	0.45 ± 0.01	7.5	648 ± 1	27.7 ± 0.6

Note. Results of single pixel H I spectral observations. VCC 190 is split into a relatively blueshifted (A) and redshifted (B) peak. Column 1: integrated flux density. Column 2: H I mass, assuming a distance of 16.7 Mpc. Column 3: heliocentric optical velocity. Column 4: full-width half maximum of Gaussian fit. For VCC 190, the fit is two simultaneous Gaussian fits, one to the narrower, low-velocity piece, and one to the wider, higher velocity tail.

et al. (2006), Oosterloo et al. (2010), and Serra et al. (2012) observed the H I in a combined 54 gas-bearing giant ellipticals in the field and the Virgo cluster. These authors found a wide range of H I morphologies, from scattered clouds and tails to regularly rotating H I disks. They infer recent or ongoing accretion as the origin of the gas when the H I is in the form of clouds, tails, and warped and disturbed disks. Oosterloo et al. (2010) also observed that star formation is generally observed in galaxies where accretion is recent or ongoing. When accretion is not recent, star formation is lacking, even when a galaxy is gas-rich.

However, the most appropriate population to compare our sample to is other low-mass early-type galaxies, such as NGC 404 and FCC046 (del Río et al. 2004; De Rijcke et al. 2013). HI has been observed in both galaxies, and attributed by the authors to gas accretion in the last gigayear. Like the more massive ellipticals, the gas in NGC 404 and FCC046 is rotating in a disk. The rotational structure of the gas is clear even in an integrated spectrum: both galaxies have classic two-horned profiles, with velocity widths of 65 km s^{-1} (del Río et al. 2004) and 67 km s^{-1} (De Rijcke et al. 2013). We note that the true rotational velocity for NGC 404 must be quite large because its HI disk is observed nearly face-on. For FCC046, the misalignment between the angular momentum of the accreted gas and the stellar component of the galaxy is very clear: the gas is in a polar ring. Like more massive ellipticals, accretion coincides with recent star formation for these dwarfs (Thilker et al. 2010; De Rijcke et al. 2013).

Whether comparing with massive or dwarf ellipticals, it is clear that accreted gas is associated with two features: the HI morphology is in the form of gas clouds, streams, or warped or disturbed disks, and the presence of star formation. For our sample—where our primary observations are single-dish spectra—the direct observable of H I in streams or disks would be a large velocity width (\gtrsim 50 km s⁻¹) or a two-horned profile as a signature of a rotating disk. We note, however, that the spectral features are not a perfect analog to resolved HI morphology and are insufficient to conclusively point to recent accretion as the source of the gas. Most notably, we would be unable to discern the existence of a warp in an otherwise smoothly rotating disk. Instead, we can argue that the lack of such features weakens the case for accretion. Neither wide velocity widths nor two-horned profiles are observed for any of the three galaxies. We do, however, observe evidence of recent star formation in VCC 611 and VCC 1533. For VCC 190,

where the H I is partially resolved, we do observe a gas tail, but we argue that gas removal is a more plausible explanation (see Section 6).

Finally, we consider the properties of free H I clouds in the Virgo cluster. Such clouds would be the source of the accreted H I in our sample. Here we run into a signficant problem. If the accretion is ongoing or recent, then a tidal interaction between the clouds and the galaxies would increase the velocity widths of the clouds' H I profiles. However, the velocity profile of the H I in each of the three galaxies is much narrower than that of any of the clouds in Virgo, which have $W_{50} \gtrsim 50 \, \mathrm{km \, s^{-1}}$ (Kent et al. 2007; Kent et al. 2009).

5.2. Between Bursts of Star Formation

The high gas fractions in our sample (see Figure 2, right) and their location at the edge of the cluster (Conselice et al. 2001; Cen et al. 2014; Jaffé et al. 2016) suggest that these galaxies are new arrivals to the cluster. However, essentially all dwarf galaxies in the field show signs of recent star formation, to varying degrees (Lee et al. 2009; Geha et al. 2012). If these galaxies were quenched prior to arriving in the cluster, then approximately 50% of their gas reservoirs could have been removed, consistent with H1 observations (Hess & Wilcots 2013; Odekon et al. 2016) and simulations (Bekki 2009; Taranu et al. 2014) of galaxy groups.

In groups, dwarfs with morphological features that are somewhere between irregulars and spheroidal dwarfs are observed (Sandage & Hoffman 1991; Mateo 1998). We observe such features in our sample: VCC 190 and VCC 1533 show deviations from a purely elliptical shape, and VCC 611 has some star-forming features at its center. Called dwarf transitionals, such galaxies have little ongoing star formation and often have detectable reservoirs of H I. The star-formation history of such galaxies was very similar to irregulars and spheroidals until roughly 1 Gyr ago (Weisz et al. 2011a, 2011b). The general interpretation is that dwarf transitionals are either between major episodes of star formation, or have simply permanently stopped forming stars (Grebel et al. 2003; Skillman et al. 2003).

The typical dwarf transitional has a lower M_* and much lower GF than our sample (Weisz et al. 2011a; De Looze et al. 2013). Our sample could be the gas-rich and more massive tail of the dwarf transitional population, holding on to more of their gas while in the group environment by virtue of their higher total mass. Indeed, our most gas-poor galaxy, VCC 611, appears in the dwarf transitional sample of De Looze et al. (2013).

⁷ We have re-fit the spectrum of FCC046 because the $W_{50} = 34 \text{ km s}^{-1}$ De Rijcke et al. (2013) report is from a Gaussian, not two-horned, fit to the spectrum.

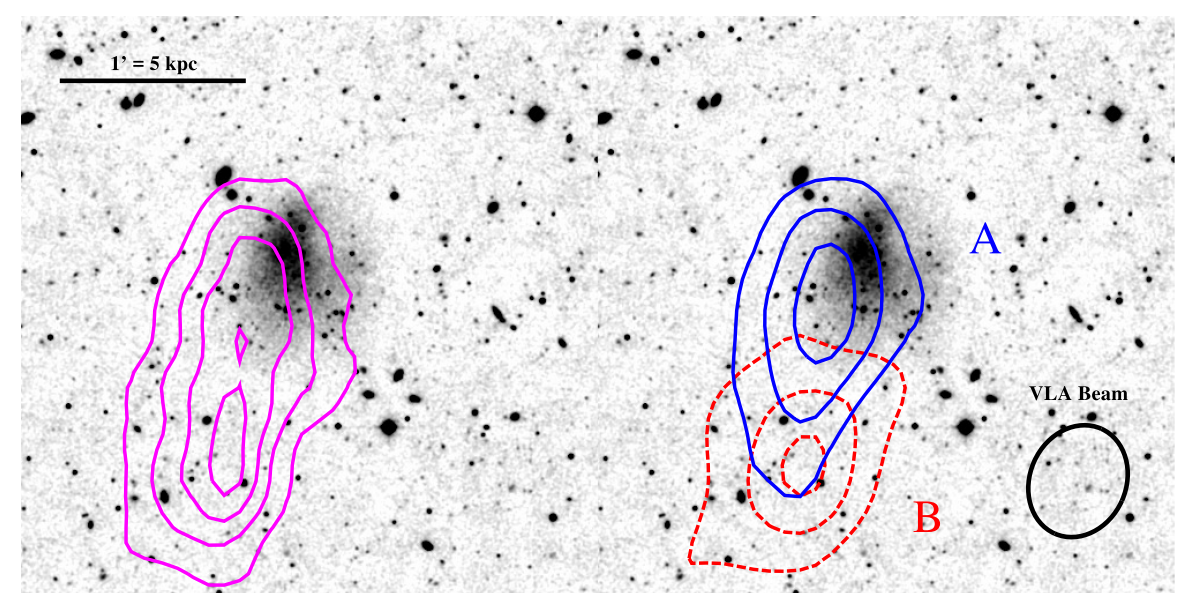


Figure 5. VLA H I intensity maps of VCC 190 overlaid on a KPNO r-band image. There are two separate reservoirs of gas in VCC 190, an undisturbed component corresponding roughly to the optical center of the galaxy, and a wide ($W_{50} = 50 \text{ km s}^{-1}$) component corresponding to the tail. Contours begin at 3σ (0.03 Jy km s⁻¹ beam⁻¹ = 0.2 M_{\odot} pc⁻²) and increase by 3σ at each additional contour. (Left) Intensity map including gas at all velocities. (Right) Because the galaxy has two distance peaks, we produce two overlaid maps, one corresponding to the blueshifted peak ($v < 2343 \text{ km s}^{-1}$; blue solid contours) and the other for the redshifted velocity peak ($v > 2343 \text{ km s}^{-1}$; red dashed contours). The lower velocity peak corresponds to gas coincident with the optical disk of the galaxy (VCC 190 A), while the higher velocity peak corresponds to an H I tail (VCC 190 B).

6. The Tail of VCC 190

Of the three galaxies in our sample, only VCC 190 has clear ongoing gas removal, as indicated by both its unusual H I spectrum and tail. The two processes most likely to produce such a tail are ram-pressure stripping and a tidal interaction with a larger galaxy or galaxies. Which is it?

Evidence for ram-pressure stripping is fairly weak. VCC 190's projected position is beyond the 3σ detection of the *ROSAT* satellite (Böhringer et al. 1994), where the effects of the ICM should be minimal. In addition, massive galaxies at this distance from the cluster center are not H I deficient, and rarely show ram-pressure stripping tails (Chung et al. 2007). However, VCC 190 is very low mass, and may be susceptible to ram-pressure stripping even when it is too weak for the more massive galaxies.

The tail geometry is also not right for ram-pressure stripping. In general, tails point opposite the motion of the galaxy, which generally means they point roughly away from the subcluster center (e.g., Chung et al. 2007; Roediger & Brüggen 2008; Kenney et al. 2014). In this case, the tail should point away from either M87 or M49, to the northwest and west, respectively, but VCC 190s tail points southwest. In addition, tails caused by stripping generally point toward the mean redshift of the cluster because the removed gas is decelerated relative to the ICM, but VCC 190's tail is blueshifted toward higher velocity.

Instead, the tidal interaction hypothesis is stronger. First, we note that the distribution of stars in VCC 190 is not a smooth ellipse, but asymmetric; the top left portion of the galaxy has a higher surface brightness than the bottom right. Ram-pressure stripping would only disturb the gas in the galaxy, while a strong tidal encounter, or multiple weaker encounters, can disturb the stars as well.

Second, it is clear which galaxies collided with VCC 190. With the exception of a few dwarf galaxies, three galaxies are within 100 kpc of VCC 190 and at a similar redshift, all to the

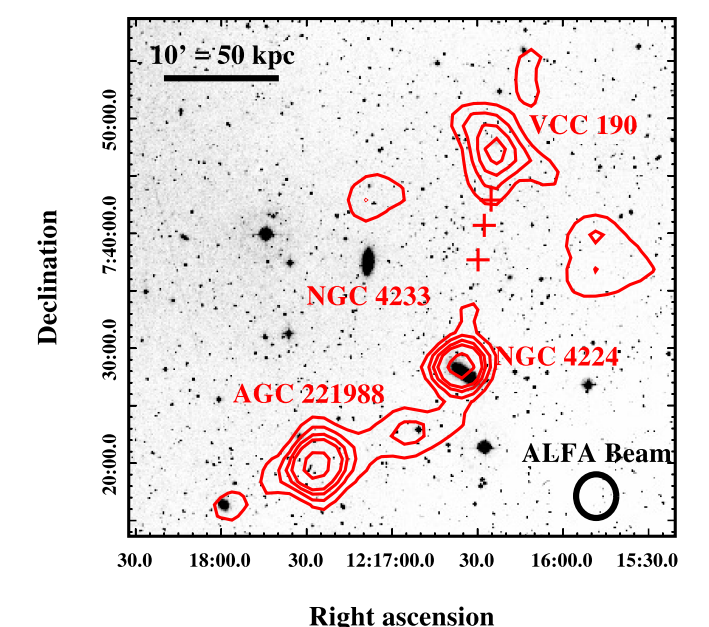


Figure 6. Environment of VCC 190. The tidal tail of VCC 190 points toward NGC 4224, suggesting a tidal encounter between the two. NGC 4224 is itself interacting with AGC 221988. Background is a DSS-2 composite optical image, while the overlaid contours are an H1 column density map; contour levels are identical to Figure 1. All galaxies with redshifts consistent with the Virgo Cluster are labeled. The red crosses are the locations of additional Arecibo pointings used to detect a bridge between NGC 4224 and VCC 190; no gas was detected at any of the three pointings.

southwest. Figure 6 shows an optical image with ALFALFA contours overlaid on these galaxies. NGC 4224 and AGC 221988 are interacting, with a tidal bridge visible between them (see Figure 6). Miskolczi et al. (2011) found stellar tidal streams coming off of NGC 4224 pointing to the north, for which they could not find an obvious interaction partner; we suggest that AGC 221988 is the cause. An optical spectrum

indicates that NGC 4233 is at the same redshift, and sthus may be interacting with the other galaxies. However, its lack of H_I means that such an interaction remains unseen in the image.

The tidal tail of VCC 190 points toward NGC 4224, suggesting an encounter between the two. In addition, NGC 4224 lies at a slightly higher redshift ($v = 2606 \,\mathrm{km \, s^{-1}}$) than VCC 190 ($v = 2345 \,\mathrm{km \, s^{-1}}$). As VCC 190 passed by NGC 4224, the removed gas in VCC 190's tail would be perturbed to a higher redshift, as is observed. We performed additional observations at Arecibo between VCC 190 and NGC 4224 (Figure 6; red crosses) to look for a tidal bridge between the two galaxies. No gas was detected, with a 3σ upper limit of $10^{6.3} \, M_{\odot}$ (0.10 Jy km s⁻¹), assuming a 30 km s⁻¹ wide tail, or approximately 5% of the H I mass of VCC 190.

Based on the disturbed and asymmetric stellar light distribution in the galaxy, the presence of a narrow and undisturbed ($W_{50} = 14 \,\mathrm{km \, s}^{-1}$) component of H I centered on the optical galaxy, and finally NGC 4224 as a clear collision partner, this tail is likely to be tidal in nature.

7. Summary

We revisited the sample of dwarf elliptical galaxies in the Virgo Cluster identified by H12. Despite being "red and dead," all had substantial reservoirs of H1 as detected in ALFALFA. We found that the two lowest signal-to-noise H1 detections reported in H12 and Haynes et al. (2011), VCC 421 and VCC 1649, were spurious. We further eliminated two more galaxies from the sample of H12: VCC 956 appears at the same sky location as a long H1 tidal tail off of NGC 4388, and VCC 1993 is not a dwarf galaxy. Our primary sample of interest was thus narrowed to three galaxies: VCC 190, VCC 611, and VCC 1533.

New radio and optical observations. High-resolution (channel width of $0.65 \, \mathrm{km \, s^{-1}}$) Arecibo observations reveal that VCC 611 and 1533 have narrow ($W_{50} < 30 \, \mathrm{km \, s^{-1}}$) velocity widths and Gaussian profiles. VCC 190 has two Gaussian peaks, one narrow and one wide ($W_{50} = 45 \, \mathrm{km \, s^{-1}}$). VLA observations of VCC 190 show an H I tail pointing toward NGC 4224 to the south, and the tail corresponds to the wide velocity feature observed at Arecibo. The ALFALFA data cubes show that NGC 4224 is interacting with one of its neighbors, AGC 221988.

Our KPNO observations and CFHT archival data from the NGVS show that all three galaxies have exponential profiles and lack widespread star-forming features. However, they do have some unusual features: the surface brightness of VCC 190 is asymmetric, VCC 611 has a star-forming feature at its center, and VCC 1533 is boxy in shape.

Elliptical morphology without significant removal of gas is observed for all three galaxies, even though gas removal in clusters should be very rapid compared with morphological change. This is supported both by their optical (exponential profiles and a lack of widespread star-forming features) and H I (narrow, undisturbed velocity profiles) features. Together, these features suggest that the galaxies are relatively new arrivals in the cluster that have not undergone significant gas stripping. We observe ongoing gas removal in VCC 190 (see below), but the current tidal interaction is too recent to be responsible for its optical properties.

These galaxies are similar to dwarf transitionals—galaxies with optical morphologies between irregulars and spheroidals with little sign of star formation. All three galaxies show some deviation

from a smooth elliptical shape; VCC 190 is asymmetrical, VCC 611 has ongoing central star formation, and VCC 1533 is box-like in shape. Transition-type dwarfs may be between bursts of star formation; our sample additionally may have been weakly stripped (<50% gas removal) while still in a group environment. Our sample is more gas-rich and has a higher M_* than is typical for dwarf transitionals (Weisz et al. 2011a; De Looze et al. 2013), and so we could be observing the most extreme galaxies in the transition population.

Ambiguous evidence for gas accretion. In elliptical galaxies with accreted gas, recent or ongoing star formation is generally observed, and the HI is in the form of clouds, streams, or a perturbed rotating disk. For two galaxies in our sample, we do observe star formation: the SDSS spectrum of VCC 611 shows strong centrally located star formation, and the overall color of VCC 1533 is at the edge of what is expected for star-forming dwarfs (NUV-r=3). With single-dish spectra, we can only imperfectly probe the HI morphology, but an HI disk will have a clear two-horned profile, and both disks and streams have wide velocity widths even in dwarfs ($W_{50} \gtrsim 50 \, \mathrm{km \, s^{-1}}$). The H I lines of VCC 611 and VCC 1533 galaxies are both narrow $(W_{50} < 30 \,\mathrm{km \, s^{-1}})$ and lack evidence of rotation because both are well-fit by a Gaussian profile. VCC 190 is not star-forming, and the H I at its optical position is similarly non-rotating. A tail is evident in H I imaging of VCC 190, but is more consistent with gas removal than accretion.

Evidence of tidal gas removal in VCC 190. An observed H I tail in VCC 190 points toward NGC 4224, while the gas coincident with the optical galaxy is practically undisturbed (fit well by a Gaussian with $W_{50} = 15 \,\mathrm{km \, s^{-1}}$). The tail is redshifted relative to the H I in the optical galaxy, as would be expected from an encounter with NGC 4224, which is at a higher redshift than VCC 190. These all suggest that the tail is a tidal feature from an encounter approximately 1 Gyr ago.

We are extremely grateful for the observations performed by the faculty and students of the Undergraduate ALFALFA Team (UAT), without which this work would not be possible. They performed the observations at Arecibo to confirm each galaxy's H I, and performed the optical observations at KPNO of VCC 190 and VCC 611. The UAT is supported by NSF grant AST-1211005.

ALFALFA has been supported by NSF grant AST-1107390, and grants from the Brinson Foundation.

This work is based in part on observations made with the Karl G. Jansky Very Large Array, a facility of the National Radio Astronomy Observatory (NRAO). The NRAO is a facility of the National Science Foundation operated under cooperative agreement by Associated Universities, Inc.

This work is based in part on observations made with the Arecibo Observatory. The Arecibo Observatory is operated by SRI International under a cooperative agreement with the National Science Foundation (AST-1100968), and in alliance with Ana G. Méndez-Universidad Metropolitana, and the Universities Space Research Association.

This work is based in part on observations made with the WIYN 0.9 m telescope operated by WIYN Inc. on behalf of a consortium of nine partner Universities and Organizations.

References

Aguerri, J. A. L., & González-García, A. C. 2009, A&A, 494, 891 Auld, R., Minchin, R. F., Davies, J. I., et al. 2006, MNRAS, 371, 1617

```
Beasley, M. A., Cenarro, A. J., Strader, J., & Brodie, J. P. 2009, AJ, 137, 5146
Begum, A., Chengalur, J. N., Karachentsev, I. D., Sharina, M. E., &
   Kaisin, S. S. 2008, MNRAS, 386, 1667
Bekki, K. 2009, MNRAS, 399, 2221
Binggeli, B., Popescu, C. C., & Tammann, G. A. 1993, A&AS, 98, 275
Binggeli, B., Sandage, A., & Tammann, G. A. 1985, AJ, 90, 1681
Binggeli, B., Tammann, G. A., & Sandage, A. 1987, AJ, 94, 251
Blanton, M. R., Kazin, E., Muna, D., Weaver, B. A., & Price-Whelan, A. 2011,
   AJ, 142, 31
Böhringer, H., Briel, U. G., Schwarz, R. A., et al. 1994, Natur, 368, 828
Boselli, A., Boissier, S., Cortese, L., & Gavazzi, G. 2008, ApJ, 674, 742
Boselli, A., Roehlly, Y., Fossati, M., et al. 2016, A&A, 596, A11
Burstein, D., Krumm, N., & Salpeter, E. E. 1987, AJ, 94, 883
Catinella, B., Schiminovich, D., Kauffmann, G., et al. 2010, MNRAS, 403, 683
Cen, R., Roxana Pop, A., & Bahcall, N. A. 2014, PNAS, 111, 7914
Chung, A., van Gorkom, J. H., Kenney, J. D. P., & Vollmer, B. 2007, ApJL,
  659, L115
Conselice, C. J., Gallagher, J. S., III, & Wyse, R. F. G. 2001, ApJ, 559, 791
Davis, T. A., Alatalo, K., Sarzi, M., et al. 2011, MNRAS, 417, 882
De Looze, I., Baes, M., Boselli, A., et al. 2013, MNRAS, 436, 1057
del Río, M. S., Brinks, E., & Cepa, J. 2004, AJ, 128, 89
De Rijcke, S., Buyle, P., & Koleva, M. 2013, ApJL, 770, L26
di Serego Alighieri, S., Gavazzi, G., Giovanardi, C., et al. 2007, A&A,
   474, 851
Dressler, A. 1980, ApJ, 236, 351
Duprie, K., & Schneider, S. E. 1996, AJ, 112, 937
Ferrarese, L., Côté, P., Cuillandre, J.-C., et al. 2012, ApJS, 200, 4
Geha, M., Blanton, M. R., Yan, R., & Tinker, J. L. 2012, ApJ, 757, 85
Giovanelli, R., Haynes, M. P., Kent, B. R., et al. 2005, AJ, 130, 2598
Grebel, E. K., Gallagher, J. S., III, & Harbeck, D. 2003, AJ, 125, 1926
Grossi, M., di Serego Alighieri, S., Giovanardi, C., et al. 2009, A&A, 498, 407
Guérou, A., Emsellem, E., McDermid, R. M., et al. 2015, ApJ, 804, 70
Hallenbeck, G., Papastergis, E., Huang, S., et al. 2012, AJ, 144, 87
Hau, G. K. T., Bower, R. G., Kilborn, V., et al. 2008, MNRAS, 385, 1965
Haynes, M. P., Giovanelli, R., & Kent, B. R. 2007, ApJL, 665, L19
Haynes, M. P., Giovanelli, R., Martin, A. M., et al. 2011, AJ, 142, 170
Hess, K. M., & Wilcots, E. M. 2013, AJ, 146, 124
Huang, S., Haynes, M. P., Giovanelli, R., et al. 2012, AJ, 143, 133
Huchtmeier, W. K., & Richter, O.-G. 1986, A&AS, 64, 111
Jaffé, Y. L., Verheijen, M. A. W., Haines, C. P., et al. 2016, MNRAS,
Kenney, J. D. P., Geha, M., Jáchym, P., et al. 2014, ApJ, 780, 119
Kent, B. R., Giovanelli, R., Haynes, M. P., et al. 2007, ApJL, 665, L15
Kent, B. R., Spekkens, K., Giovanelli, R., et al. 2009, ApJ, 691, 1595
Koleva, M., de Rijcke, S., Prugniel, P., Zeilinger, W. W., & Michielsen, D.
   2009, MNRAS, 396, 2133
Koopmann, R. A., & Kenney, J. D. P. 2004, ApJ, 613, 866
```

```
Lee, J. C., Kennicutt, R. C., Jr., Funes, S. J. J. G., Sakai, S., & Akiyama, S.
  2009, ApJ, 692, 1305
Lisker, T., Glatt, K., Westera, P., & Grebel, E. K. 2006a, AJ, 132, 2432
Lisker, T., Grebel, E. K., & Binggeli, B. 2006b, AJ, 132, 497
Lisker, T., Weinmann, S. M., Janz, J., & Meyer, H. T. 2013, MNRAS,
   432, 1162
Mateo, M. L. 1998, ARA&A, 36, 435
Mayer, L., Governato, F., Colpi, M., et al. 2001, ApJ, 559, 754
Mei, S., Blakeslee, J. P., Côté, P., et al. 2007, ApJ, 655, 144
Meyer, H. T., Lisker, T., Janz, J., & Papaderos, P. 2014, A&A, 562, A49
Miskolczi, A., Bomans, D. J., & Dettmar, R.-J. 2011, A&A, 536, A66
Mistani, P. A., Sales, L. V., Pillepich, A., et al. 2016, MNRAS, 455, 2323
Morganti, R., de Zeeuw, P. T., Oosterloo, T. A., et al. 2006, MNRAS, 371, 157
Odekon, M. C., Koopmann, R. A., Haynes, M. P., et al. 2016, ApJ, 824, 110
Oosterloo, T., Morganti, R., Crocker, A., et al. 2010, MNRAS, 409, 500
Oosterloo, T., & van Gorkom, J. 2005, A&A, 437, L19
Paudel, S., Lisker, T., Kuntschner, H., Grebel, E. K., & Glatt, K. 2010,
        AS, 405, 800
Penny, S. J., Forbes, D. A., Pimbblet, K. A., & Floyd, D. J. E. 2014, MNRAS,
  443, 3381
Rakos, K., & Schombert, J. 2004, AJ, 127, 1502
Roediger, E., & Brüggen, M. 2008, MNRAS, 388, 465
Roediger, J. C., Courteau, S., MacArthur, L. A., & McDonald, M. 2011,
   MNRAS, 416, 1996
Ryś, A., Falcón-Barroso, J., & van de Ven, G. 2013, MNRAS, 428, 2980
Sandage, A., & Hoffman, G. L. 1991, ApJL, 379, L45
Serra, P., Oosterloo, T., Morganti, R., et al. 2012, MNRAS, 422, 1835
Skillman, E. D., Côté, S., & Miller, B. W. 2003, AJ, 125, 593
Struve, C., Oosterloo, T., Sancisi, R., Morganti, R., & Emonts, B. H. C. 2010,
  A&A, 523, A75
Taranu, D. S., Hudson, M. J., Balogh, M. L., et al. 2014, MNRAS, 440,
Taylor, R., Davies, J. I., Auld, R., & Minchin, R. F. 2012, MNRAS, 423,
Thilker, D. A., Bianchi, L., Schiminovich, D., et al. 2010, ApJL, 714,
  L171
Toloba, E., Boselli, A., Cenarro, A. J., et al. 2011, A&A, 526, A114
Toloba, E., Guhathakurta, P., Peletier, R. F., et al. 2014, ApJS, 215, 17
Toloba, E., Li, B., Guhathakurta, P., et al. 2016, ApJ, 822, 51
van Zee, L., Skillman, E. D., & Haynes, M. P. 2004, AJ, 128, 121
Weinmann, S. M., Lisker, T., Guo, Q., Meyer, H. T., & Janz, J. 2011, MNRAS,
  416, 1197
Weisz, D. R., Dalcanton, J. J., Williams, B. F., et al. 2011a, ApJ, 739, 5
Weisz, D. R., Dolphin, A. E., Dalcanton, J. J., et al. 2011b, ApJ, 743, 8
Weisz, D. R., Dolphin, A. E., Skillman, E. D., et al. 2014, ApJ, 789, 147
Yıldız, M. K., Serra, P., Peletier, R. F., Oosterloo, T. A., & Duc, P.-A. 2017,
   MNRAS, 464, 329
```